Mineralogia, vol. 53, 2022, 10-19 *Original Paper*

DOI: 10.2478/mipo-2022-0002

High temperature transformation of iron-bearing minerals in basalt: Mössbauer spectroscopy studies

Mariola Kądziołka-Gaweł[1]*

Marcin Wojtyniak[2]

Joanna Klimontko[1]

[1]Institute of Physics, University of Silesia, 75 Pułku Piechoty 1, 41-500 Chorzów, Poland
[2]Institute of Physics, Silesian University of Technology, Konarskiego 22B, 44-100 Gliwice, Poland
*Corresponding author: mariola.kadziolka-gawel@us.edu.pl

Abstract

The high temperature decomposition of basalt from Lower Silesia (Poland) was followed by Mössbauer spectroscopy investigation. The Fe content of the sample was ~9.0 at.%. The X-ray diffraction analysis shows that augite (37%) and olivine (12%) are major Fe-bearing mineral components. The sample also contains significant amount of anorthite (22%) and nepheline (17%). The sample was heated at various temperatures between 200°C and 1100°C for three hours. Up to a temperature of 500°C changes in contribution of Fe-bearing minerals are insignificant. Heating in the temperature range from 500°C to 1100°C leads to a systematic increase in contribution of iron oxides at the cost of contribution of silicate minerals, like augite and olivine. Mössbauer spectrum obtained after heating at 1100°C showed hematite as the main iron oxide phase. The ratio of Fe^{3+}/Fe_{tot} in the non-heated sample was equal to 0.51 and after heating at 1100°C this ratio amounted to 0.89.

Keywords: basalts; high temperature affects; Mössbauer spectroscopy; Fe-bearing minerals.

1. Introduction

Basalt is the name given to a wide variety of volcanic rocks, known principally for its resistance to high temperatures, strength, durability, and wide distribution around the world. Basalt rock forms when lava erupts at the Earth's surface for example at mid ocean ridges. The lava is between 1100°C to 1250°C when it is erupted and it cools quickly to form solid rock, within a few days or a couple of weeks (Sedlačková et al. 2021). The specific gravity of basalt is nearly 3 g/cm^3 (Al-Baijat, Benedetti 2013; Mishra et al. 2018) and it can be extremely hard, ranging from *5* to 9 on Mohs' scale (Felippi de Lima et al. 2022). For these reasons it is often used in its natural form as paving and building stone. Furthermore, the good mechanical properties of basalt and basalt rock products like basalt rebars (Urbanski et al. 2013), basalt fabrics, chopped basalt fiber strands (Liu et al. 2006; Monaldo et al. 2019), continuous basalt filament wires or basalt mesh (Sunny et al. 2020), make them particularly suitable for many industrial applications, including building materials and thermal insulators.

Almost all industrial processes in which basalt is used are thermal processes. Annealing of basalt causes a

number of changes in its mineralogical composition, structure and physical properties. Basalt is mainly composed of silicate minerals, where iron is one of the main elements. It is well known that the Mössbauer spectroscopy method (Stucki et al. 1988) is very sensitive to the local atomic structure, deformation, atomic or lattice defects and can provide quantitative information concerning iron atoms in geological samples. Currently, there are many investigations into the physiochemical properties and application performance of basalt products. There several studies of basalts characterized by Mössbauer spectroscopy (Gunnlaugsson et al. 2008; Thompson et al. 2011; Hassan, Dekan 2013; Malczewski et al. 2017). However, reports on Mössbauer studies of basalt after heating in air are relatively uncommon (Burkhard 2001). Therefore, our objectives were to study high temperature changes in different fractions of basalt after heating in air by ^{57}Fe Mössbauer, X-ray diffraction and X-ray fluorescence methods. The results, in turn, enhance our knowledge of the physiochemical properties of basalt, a widely used material in many industry applications.

2. Samples and methods

A composite sample of Tertiary basalt from the Lower Silesia region (Wilków, Pogórze Kaczawskie, SW Poland), which forms the eastern part of the Central European Volcanic Province was kindly provided by PGP "BAZALT" SA. This rock mine is opencast. The sample is a mixture of basalt chunks that represent an average sample from the region. These samples are dark grey and without fail contain olivine phenocrysts, which were recognized with the naked eye. The material was divided into seven groups with different granulation (0-0.063 mm, 0-2 mm, 2-5 mm, 4-8 mm, 8-11 mm, 11-16 mm and 16-22 mm). The sample with 0-2 mm granulation was heated for three hours in an electric furnace in atmosphere air under static conditions in a temperature range from 200°C to 1100°C. After each heating treatment, the Mössbauer measurement was taken.

The chemical composition of all samples were determined by X-ray fluorescence (XRF) with a ZSX Primus II Rigaku spectrometer at the University of Silesia (Institute of Physics). The spectrometer, equipped with the 4 kW, 60 kV Rh anode and wavelength dispersion detection system, allowed for the analysis of the elements from Be to U. No external standards were necessary, only the internal standards coupled with the fundamental parameters (theoretical relationship between the measured X-ray intensities and the concentrations of elements in the sample) were implemented. The samples for the analysis were prepared in the form of pressed tablets.

To identify minerals present in investigated sample, X-ray diffraction studies were done (XRD). These studies were conducted at room temperature by the use of a Siemens D5000 Xray diffractometer and CuK_{α} radiation at the University of Silesia (Institute of Physics). Rietveld refinement was performed in a licensed Xpert High Score Plus with a PDF-4 crystallography database. The phase content is assumed to be less than 2% in volume. Main sources of errors are the background, orientation of phyllosilicates or grinding of the samples.

^{57}Fe Mössbauer transmission spectra were recorded at room temperature with an MS96 Mössbauer spectrometer and a linear arrangement of a ^{57}Co:Rh source, a multichannel analyser with 1024 channels (before folding), an absorber and a detector. The spectrometer was calibrated at room temperature with a 30 mm thick αFe foil. Numerical analysis of the Mössbauer spectra was performed by means of the WMOSS program (Ion Prisecaru, WMOSS4 Mössbauer Spectral Analysis Software, 2009-2016).

3. Results

Figure 1 presents contents of the elements in the investigated basalts with different granulation. The results indicated that chemical composition of all the investigated samples is almost the same and virtually does not depend on the granulation. The analysed

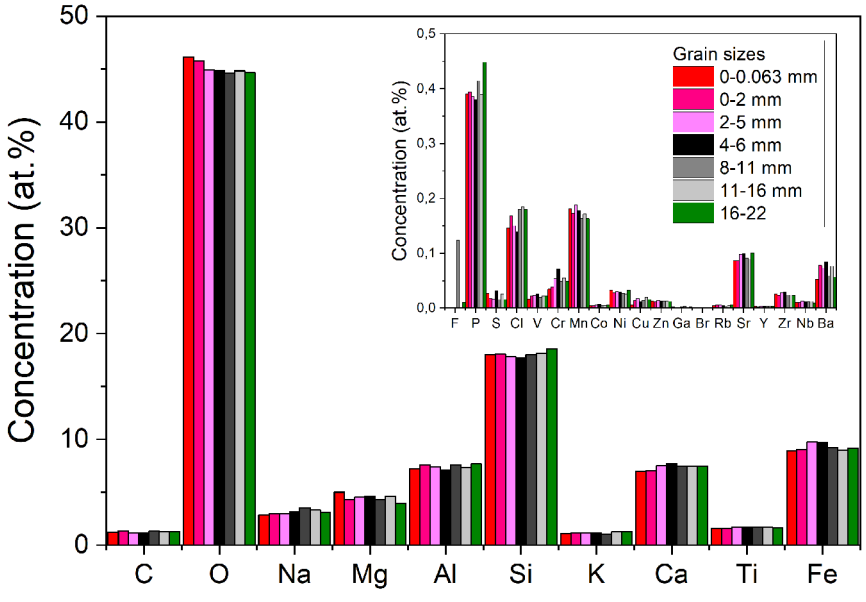

Figure 1. Elements concentrations higher than 1 at.% and smaller than 1 at.% (insert) of the investigated samples with different grain sizes. In the graph the Y-axis concentration (at.%).

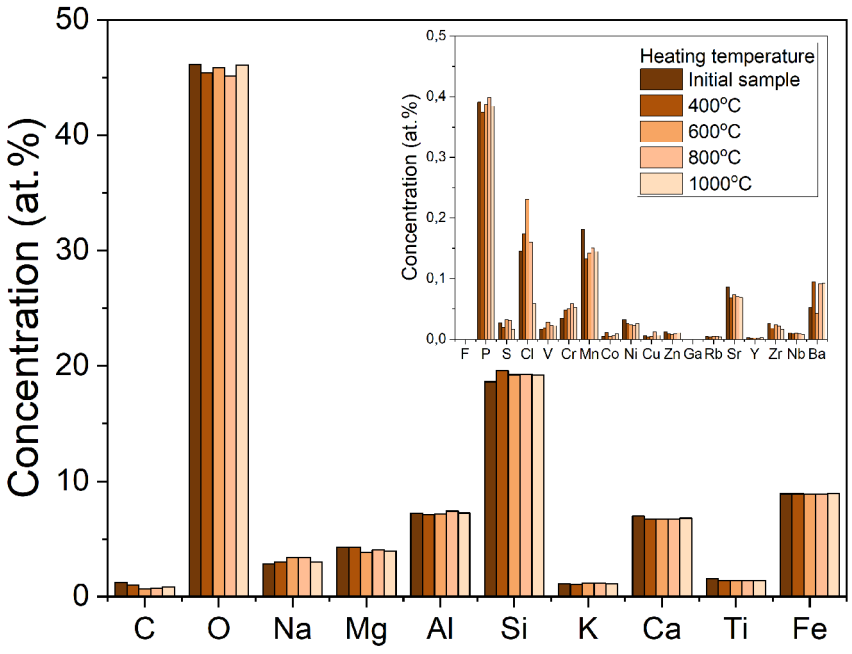

Figure 2. Elements concentrations of the 0-2 mm size fraction of the basalt before and after heat treatment. In the graph the Y-axis concentration (at.%).

materials contained very small amounts of Cr (~0.05 at.%), Zn (~0.01 at.%), Cu (~0.01 at.%), Ti (~1.66 at.%), Sr (~0.11 at.%) and Ba (~0.07 at.%), accompanied by large amounts of Si (~18.04 at.%), Fe (~9.26 at.%), Al (~7.42 at.%), Ca (~7.38 at.%), Mg (~4.49 at.%) and Na (~3.12 at.%), which, just as C and O, are elements of minerals present in basalt rocks. The variability of the element concentrations in the analysed 0-2 mm sample during heating in air are shown in Figure 2. The measured concentrations were almost constant, reflecting that present minerals have much higher melting temperatures than the highest applied heating temperature (i.e. 1100 °C).

Figure 3 presents X-ray diffraction patterns the 0-2 mm sample before and after heating at selected temperatures (400°C, 600°C, 800°C and 1000°C). Mineral composition for the investigated sample of the basalt obtained during heating process is listed in Table 1. The results of the mineralogical analysis of this non-heated sample show that augite $(Al,Ca,Fe,Mg,Ti)_2(Al,Si)_2O_6$ (37%), anorthite $CaAl_2Si_2O_8$ (22%), nepheline $(Na,K)AlSiO_4$ (18%) and olivine $(Mg,Fe)_2SiO_4$ (12%) are major mineral components. Magnesioferrite $MgFe_2O_4$ (7%), goethite α-FeOOH (3%) and sodalite $Na_8Al_6Si_6O_{24}Cl_2$ (2%) are minor components. Structural changes were not observed up to temperature 400°C. However, after heating the sample at temperature 600°C diffraction lines related to hematite are visible. The line with the highest intensity for hematite is placed at 2Θ=33.2°. Its intensity increase with increasing of heating temperature. X-ray diffraction analysis show that most of the diffraction lines visible for non-heated sample are also present after heating at temperature 1000°C. Line intensities for augite, anorthite, nepheline or olivine decrease whereas those connected with hematite and magnesioferrite increase. Based on these results we can assume that concentration of iron oxides increases or some part of aluminosilicates and silicates lose crystalline form and generate subcrystallite domains, which give low intensity diffraction lines.

Mössbauer spectra of all samples are presented on Figure 4. The spectra consist of components related to iron-bearing phases with different content and their hyperfine parameters are listed in Table 2. They are best fitted as four sextets and five doublets. The sextets with hyperfine magnetic fields of about 43 T and 38 T are connected with magnesioferrite and result from Fe^{3+} on the tetrahedral sites and Fe^{3+} on the octahedral sites of the spinel structure respectively. The isomer shifts at both sites are of comparable values that indicates similar covalence effects of Fe^{3+} ions at both sites (Lakshman et al. 2004). Additionally, the broadening of the lines in magnesioferrite has been interpreted as being due to the distribution of magnetic hyperfine fields caused by the random occupancy of the tetrahedral and octahedral sites by Fe^{3+}, Mg^{2+} or other cations, which can substitute them. The hyperfine magnetic fields of 31 T and 23 T are associated with goethite. The broadness of the sextet lines can be a result of poorly ordered goethite (Komadel et al. 2008). Additionally, natural conditions include mineral phases with the com-

Table 1. Mineral composition (in %vol) for the 0-2 mm size fraction of the basalt obtained during heating process.

Component	Formula	Heating temperature				
		Row	400°C	600°C	800°C	1000°C
Augite	$(CaFeMg)_2Si_2O_6$	37	37	35	29	26
Anorthite	$CaAl_2Si_2O_8$	22	23	25	26	23
Nepheline	$(K, Na)AlSiO_4$	18	17	15	16	13
Olivine	$(Mg, Fe)_2SiO_4$	12	12	12	11	12
Magnesioferrite	$MgFe_2O_4$	7	7	4	5	7
Goethite	FeOOH	3	3	-	-	-
Sodalite	$Na_8(Al_2Si_6O_{24})Cl_2$	2	2	3	3	2
Hematite	Fe_2O_3	-	-	5	6	8
Quartz	SiO_2	-	-	1	4	7

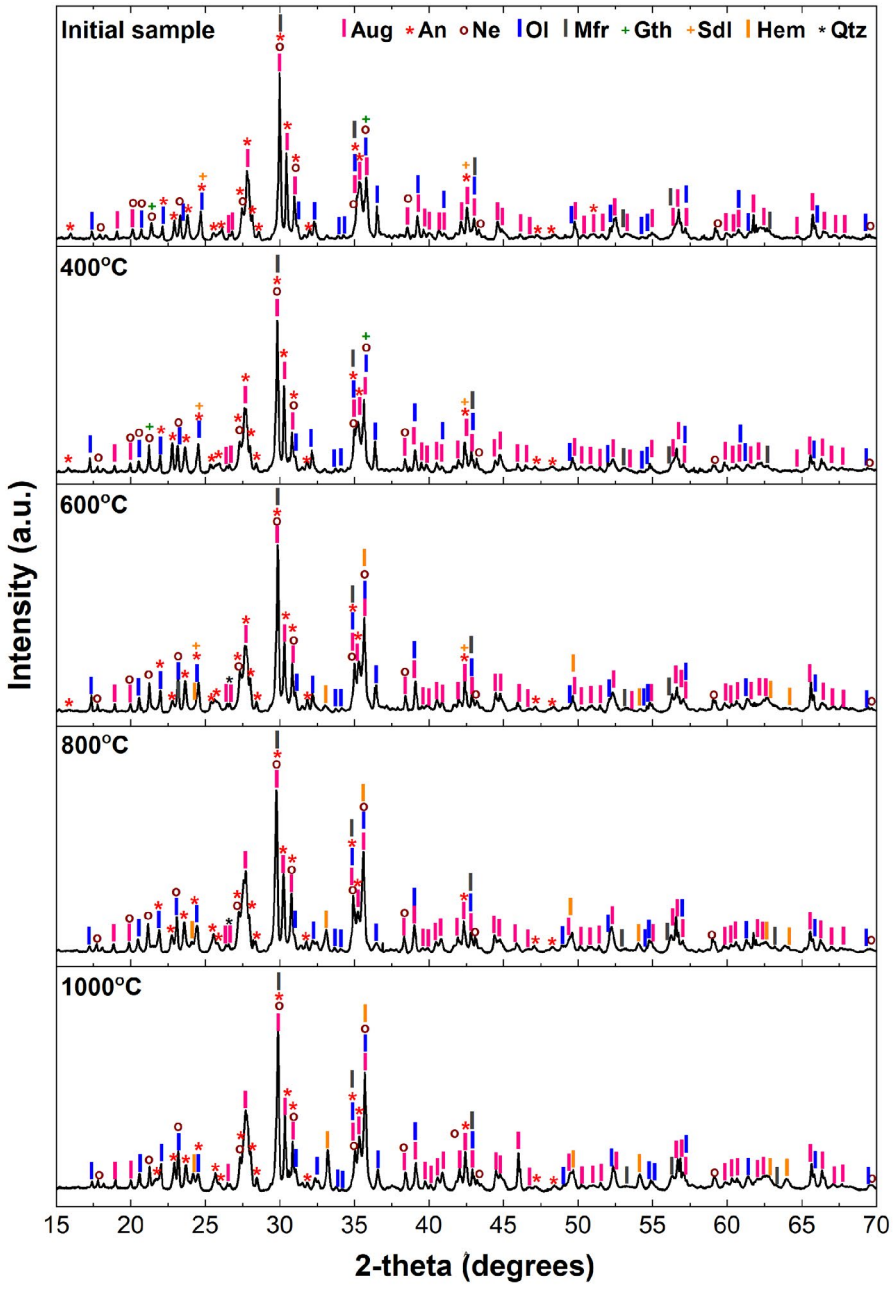

Figure 3. XRD patterns of the 0-2 mm size fraction of the basalt before and after heat treatment. Identified peaks are: Augite (Aug), Anorthite (An), Nepheline (Ne), Olivine (Ol), Magnesioferrite (Mfr), Goethite (Gth), Sodalite (Sdl) and Quartz (Qtz).

position differing from the stoichiometric variety due to vacancy mechanism and isomorphic replacement mechanism. Therefore, the hyperfine magnetic fields obtained for these Feoxides and hydroxides are lower than those reported in the literature (Stevens et al. 2005; Hassan 2015). The two doublets with isomer shift (IS) values of 1.06–1.21 mm/s and quadrupole splitting (QS) of 2.55–2.85 mm/s and 2.88-2.95 mm/s originate with Fe^{2+} ions in the octahedral positions of the olivine structure (Kądziołka-Gaweł et al. 2018). The doublet with the smaller quadrupole splitting, i.e. the larger distortion of the corresponding octahedron, can be assigned to Fe^{2+} in octahedron labeled as M1, the other one with the larger quadrupole splitting to Fe^{2+} in octahedron labeled as M2 (Morozov et al. 2005). Three other doublets can be assigned to Fe ions located in augite structure. Augite is an essential mineral in basalts and belongs to the pyroxenes (Morimoto 1988; Dyar et al. 2013). First of them has QS values varying from 0.62 to 0.67 mm/s and IS values varying from 0.47 to 0.53 mm/s. Hyperfine parameters of this component indicate Fe^{3+} ions in octahedral coordination. These ions constitute about 65% of iron in augite and about 25% of iron in all the samples (Table 1). Two other doublets with IS from 0.92-1.06 mm/s and QS from 1.80-2.18 mm/s are connected with octahedrally coordinated Fe^{2+} ions also in augite.

Figure 5 shows room temperature Mössbauer spectra obtained for the sample heated up to a temperature of 1100°C, while the changes in concentration of silicates, Fe-oxides/hydroxides and ratio of Fe^{3+} to total iron (Fe_{tot}) obtained after heating at high temperatures are presented in Figure 6. Obtained hyperfine parameters for all fitted components are listed in Table 3. A decrease in contribution of goethite is observed after heating the sample at 500°C. Mössbauer spectrum obtained after heating at 1100°C showed hematite as the main iron oxide phase.

4. Discussion

The XRF results indicate the Fe content of the sample was 9.03 at.%. The X-ray diffraction analysis shows that augite and olivine are major Fe-bearing mineral components and magnesioferrite and goethite are minor components in row basalt samples. Results of these methods also show that after heating the sample above 1000°C augite and hematite are the main Fe-bearing components. Elements concentrations did not depend of sample granulation and on heating temperature up to 1000°C. The structure and element concentration of these materials determines their durability. Above basalt properties can be essentially used in many fields of civil engineering. Additionally, relative homogeneous chemical structure and large-scale availability make basalt an excellent raw material for fiber-forming (Sunny et al. 2020).

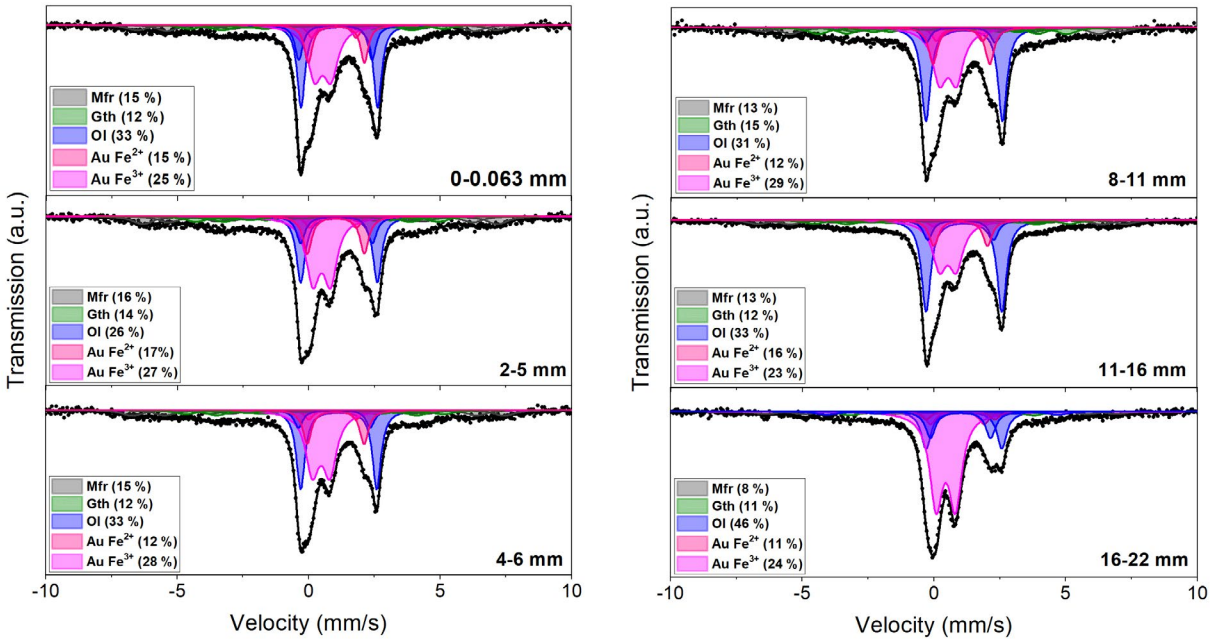

Figure 4. Mössbauer spectra obtained for basalts with different granulation. Fitted components, their assignment (Au – augite, Ol – olivine, Mfr – magnesioferrite, Gth – goethite) and concentration are indicated on the spectra.

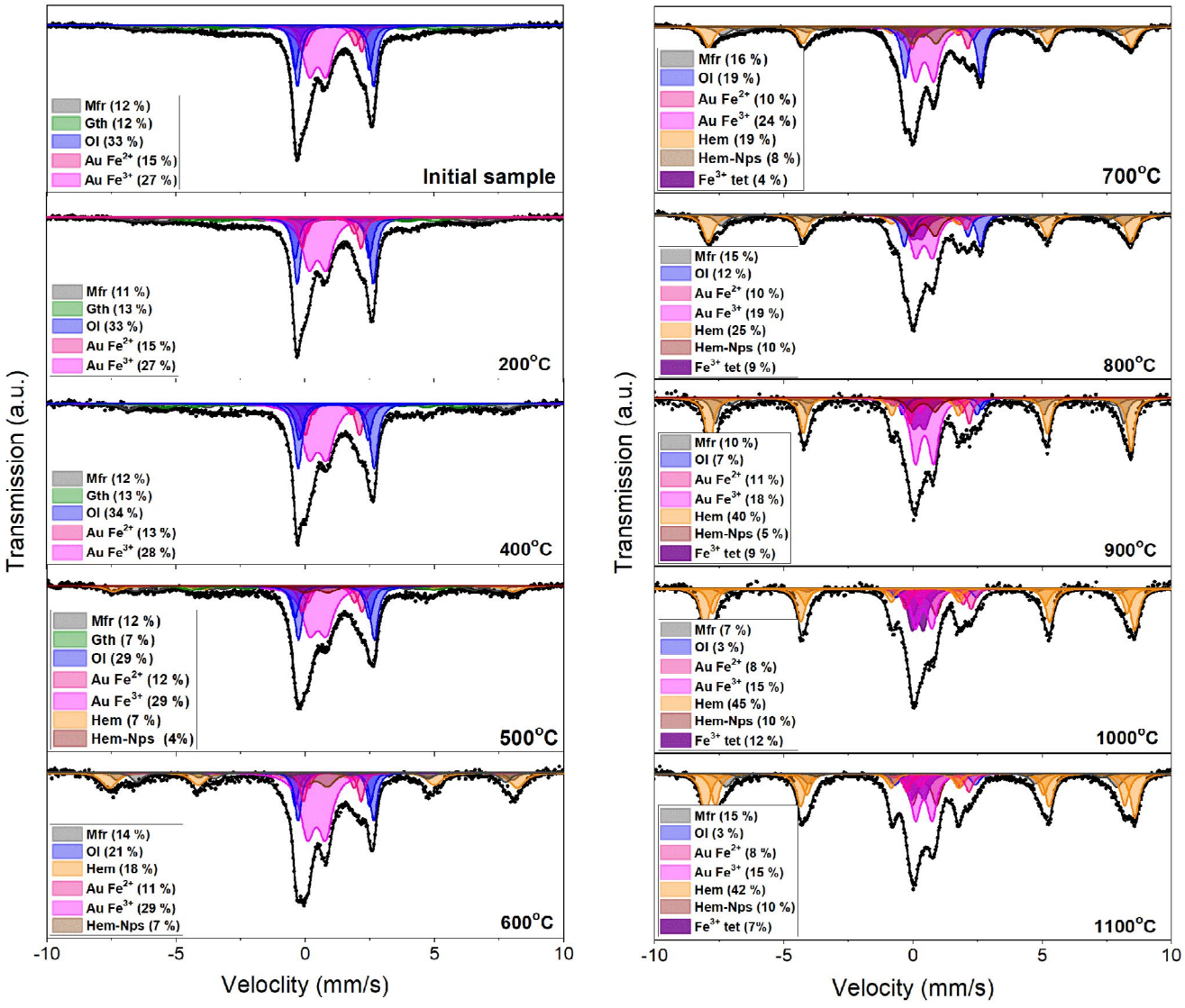

Figure 5. Room temperature Mössbauer spectra obtained after heating of basalt sample at selected temperatures. Fitted sub-spectra and their assignments are visible on the spectra.

Table 2. Hyperfine parameters: isomer shift (IS), quadrupole splitting (QS), hyperfine magnetic field (H), line width (G), relative peak areas (A) and components asigments of spectral components from the Mössbauer spectra obtained for the raw basalt samples. IS, QS and G are in mm/s; A is in percent and H is in T. Estimated errors are ± 0.02 mm/s for IS, QS and G; ± 0.5 T for H, and ± 1% for A.

	IS	QS	H	G	A	Component		IS	QS	H	G	A	Component
0-0.063 mm	0.49	0.66	-	0.60	26	Fe^{3+} Au	8-11 mm	0.52	0.64	-	0.65	25	Fe^{3+} Au
	0.98	1.88	-	0.35	5	Fe^{2+} Au		0.96	1.75	-	0.40	4	Fe^{2+} Au
	1.04	2.28	-	0.35	10	Fe^{2+} Au		1.03	2.16	-	0.40	11	Fe^{2+} Au
	1.05	2.87	-	0.35	12	Fe^{2+} Ol		1.01	2.66	-	0.40	4	Fe^{2+} Ol
	1.17	2.95	-	0.35	20	Fe^{2+} Ol		1.14	2.91	-	0.40	27	Fe^{2+} Ol
	0.30	0.00	42.2	0.80	7	Fe^{3+} Mfr		0.30	0.00	42.6	0.85	5	Fe^{3+} Mfr
	0.38	0.00	36.9	0.80	7	Fe^{3+} Mfr		0.39	0.00	36.6	0.85	8	Fe^{3+} Mfr
	0.37	-0.14	22.6	0.85	7	Fe^{3+} Gth		0.37	-0.12	22.7	0.85	7	Fe^{3+} Gth
	0.37	-0.15	29.5	0.85	6	Fe^{3+} Gth		0.37	-0.11	29.4	0.85	8	Fe^{3+} Gth
2-5 mm	0.49	0.67	-	0.60	27	Fe^{3+} Au	11-16 mm	0.53	0.63	-	0.65	24	Fe^{3+} Au
	0.92	1.77	-	0.40	4	Fe^{2+} Au		0.85	1.70	-	0.40	3	Fe^{2+} Au
	1.06	2.13	-	0.40	11	Fe^{2+} Au		1.02	2.07	-	0.40	9	Fe^{2+} Au
	1.05	2.87	-	0.40	9	Fe^{2+} Ol		1.03	2.54	-	0.40	7	Fe^{2+} Ol
	1.15	2.92	-	0.40	19	Fe^{2+} Ol		1.14	2.88	-	0.40	32	Fe^{2+} Ol
	0.38	0.00	42.1	0.80	9	Fe^{3+} Mfr		0.30	0.00	43.3	0.80	6	Fe^{3+} Mfr
	0.43	0.00	36.1	0.80	7	Fe^{3+} Mfr		0.44	0.00	36.9	0.80	7	Fe^{3+} Mfr
	0.37	-0.12	22.2	0.85	7	Fe^{3+} Gth		0.37	-0.12	22.7	0.85	6	Fe^{3+} Gth
	0.37	-0.11	28.8	0.85	7	Fe^{3+} Gth		0.37	-0.13	30.3	0.85	6	Fe^{3+} Gth
4-6 mm	0.48	0.67	-	0.62	29	Fe^{3+} Au	16-22 mm	0.45	0.73	-	0.60	46	Fe^{3+} Au
	0.90	1.82	-	0.38	3	Fe^{2+} Au		0.89	1.99	-	0.40	5	Fe^{2+} Au
	1.03	2.17	-	0.38	10	Fe^{2+} Au		1.11	2.29	-	0.40	11	Fe^{2+} Au
	1.01	2.75	-	0.38	6	Fe^{2+} Ol		1.01	2.61	-	0.40	4	Fe^{2+} Ol
	1.15	2.90	-	0.38	23	Fe^{2+} Ol		1.11	2.88	-	0.40	15	Fe^{2+} Ol
	0.36	0.00	43.9	0.80	8	Fe^{3+} Mfr		0.30	0.00	41.3	0.85	4	Fe^{3+} Mfr
	0.44	0.00	36.8	0.80	8	Fe^{3+} Mfr		0.44	0.00	36.1	0.85	4	Fe^{3+} Mfr
	0.37	-0.12	23.7	0.85	7	Fe^{3+} Gth		0.37	-0.12	21.7	0.85	6	Fe^{3+} Gth
	0.37	-0.18	30.6	0.85	6	Fe^{3+} Gth		0.37	-0.11	28.3	0.85	5	Fe^{3+} Gth

There are no significant changes in contribution of components visible on Mössbauer spectra of the sample heated up to a temperature of 400°C (Figure 5, Table 3). A decrease in contribution of goethite is observed after heating the sample at 500°C and on the Mössbauer spectrum appears a sextet with hyperfine magnetic field of 48.5 T associated with hematite Fe_2O_3. Dehydration of goethite involves removal of hydrogen and one quarter of the oxygen, without disturbing the network of the remaining oxygen, and atomic rearrangement of Fe^{3+} to form hematite (Özdemir, Dunlop 2000; Gialanella et al. 2010). After heating the sample at 600°C sextets related to goethite are not visible. Additionally, the result of annealing the sample at 500°C is appearance of ferric doublet with hyperfine parameters IS = 0.41 mm/s and QS = 0.92 mm/s on Mössbauer spectrum. This component can be related to the formation of superparamagnetic nanoparticles of Fe_2O_3 (Brown et al. 1998; Barcova et al. 2003; Rivas-Sanchez et al. 2009) as a result of oxidation of Fe^{2+} ions in the olivine structure (Kądziołka-Gaweł et al. 2019). It indicates that the decomposition of the olivine structure starts at this temperature. This process

Table 3. Hyperfine parameters and relative peak areas of spectral components from the Mössbauer spectra obtained for the 0-2 mm size fraction of the basalt before and after heating at high temperatures (T). The meaning of the parameters and errors are the same as in Table 2.

T	IS	QS	H	G	A	Component	T	IS	QS	H	G	A	Component
Initial sample	0.49	0.66	-	0.62	27	Fe^{3+} Au	700°C	0.44	0.70	-	0.55	24	Fe^{3+} Au
	0.98	1.88	-	0.34	5	Fe^{2+} Au		1.03	1.47	-	0.32	3	Fe^{2+} Au
	1.04	2.28	-	0.34	10	Fe^{2+} Au		1.04	2.15	-	0.32	7	Fe^{2+} Au
	1.05	2.87	-	0.34	13	Fe^{2+} Ol		0.95	2.78	-	0.32	4	Fe^{2+} Ol
	1.17	2.95	-	0.34	21	Fe^{2+} Ol		1.15	2.93	-	0.32	15	Fe^{2+} Ol
	0.30	0.00	42.1	0.80	5	Fe^{3+} Mfr		0.38	0.00	48.1	0.60	10	Fe^{3+} Mfr
	0.42	0.00	36.8	0.80	7	Fe^{3+} Mfr		0.59	0.00	44.6	0.60	6	Fe^{3+} Mfr
	0.37	-0.12	22.6	0.85	6	Fe^{3+} Gth		0.37	-0.21	50.9	0.50	19	Fe^{3+} Hem
	0.37	-0.15	29.5	0.85	6	Fe^{3+} Gth		0.43	0.91	-	0.55	8	Fe^{3+}
								0.16	0.45	-	0.55	4	Fe^{3+}
200°C	0.47	0.62	-	0.65	27	Fe^{3+} Au	800°C	0.43	0.65	-	0.52	19	Fe^{3+} Au
	0.99	1.80	-	0.35	5	Fe^{2+} Au		1.06	1.44	-	0.34	3	Fe^{2+} Au
	1.05	2.18	-	0.35	10	Fe^{2+} Au		1.06	2.14	-	0.34	7	Fe^{2+} Au
	1.03	2.80	-	0.35	13	Fe^{2+} Ol		1.00	2.68	-	0.34	2	Fe^{2+} Ol
	1.19	2.89	-	0.35	21	Fe^{2+} Ol		1.14	2.94	-	0.34	10	Fe^{2+} Ol
	0.35	0.00	43.2	0.85	4	Fe^{3+} Mfr		0.38	0.00	48.4	0.50	11	Fe^{3+} Mfr
	0.38	0.00	38.5	0.85	7	Fe^{3+} Mfr		0.50	0.00	44.6	0.50	4	Fe^{3+} Mfr
	0.37	-0.12	25.6	0.85	7	Fe^{3+} Gth		0.37	-0.21	50.9	0.47	25	Fe^{3+} Hem
	0.37	-0.14	32.5	0.85	6	Fe^{3+} Gth		0.37	0.92	-	0.52	10	Fe^{3+}
								0.16	0.40	-	0.52	9	Fe^{3+}
400°C	0.49	0.68	-	0.65	28	Fe^{3+} Au	900°C	0.45	0.64	-	0.50	16	Fe^{3+} Au
	1.05	1.53	-	0.35	3	Fe^{2+} Au		1.10	1.49	-	0.37	3	Fe^{2+} Au
	1.06	2.09	-	0.35	10	Fe^{2+} Au		1.07	2.21	-	0.37	6	Fe^{2+} Au
	1.10	2.67	-	0.35	12	Fe^{2+} Ol		1.09	2.91	-	0.37	7	Fe^{2+} Ol
	1.16	2.98	-	0.35	22	Fe^{2+} Ol		0.36	0.00	47.7	0.50	9	Fe^{3+} Mfr
	0.38	0.00	45.5	0.85	5	Fe^{3+} Mfr		0.34	0.00	43.6	0.50	3	Fe^{3+} Mfr
	0.42	0.00	40.0	0.85	7	Fe^{3+} Mfr		0.37	-0.20	50.5	0.40	40	Fe^{3+} Hem
	0.37	-0.10	28.0	0.85	7	Fe^{3+} Gth		0.40	0.91	-	0.50	7	Fe^{3+}
	0.37	-0.18	35.4	0.85	6	Fe^{3+} Gth		0.17	0.49	-	0.50	9	Fe^{3+}
500°C	0.48	0.64	-	0.60	29	Fe^{3+} Au	1000°C	0.41	0.64	-	0.40	15	Fe^{3+} Au
	1.00	1.81	-	0.40	3	Fe^{2+} Au		1.10	1.67	-	0.36	3	Fe^{2+} Au
	1.05	2.27	-	0.40	9	Fe^{2+} Au		0.98	2.41	-	0.36	5	Fe^{2+} Au
	1.03	2.88	-	0.40	11	Fe^{2+} Ol		0.90	2.99	-	0.36	3	Fe^{2+} Ol
	1.19	2.93	-	0.40	18	Fe^{2+} Ol		0.31	0.00	47.7	0.50	5	Fe^{3+} Mfr
	0.39	0.00	43.6	0.70	5	Fe^{3+} Mfr		0.42	0.00	46.1	0.50	2	Fe^{3+} Mfr
	0.40	0.00	38.8	0.70	7	Fe^{3+} Mfr		0.37	-0.21	51.8	0.40	29	Fe^{3+} Hem
	0.37	-0.12	48.3	0.70	7	Fe^{3+} Hem		0.37	-0.22	49.9	0.40	16	Fe^{3+} Hem
	0.37	-0.14	29.1	0.85	7	Fe^{3+} Gth		0.41	0.90	-	0.40	10	Fe^{3+}
	0.41	0.91	-	0.40	4	Fe^{3+}		0.19	0.44	-	0.40	12	Fe^{3+}
600°C	0.42	0.70	-	0.65	30	Fe^{3+} Au	1100°C	0.41	0.64	-	0.40	15	Fe^{3+} Au
	1.02	1.76	-	0.32	3	Fe^{2+} Au		1.10	1.50	-	0.39	3	Fe^{2+} Au
	1.04	2.24	-	0.32	7	Fe^{2+} Au		0.96	2.41	-	0.39	5	Fe^{2+} Au
	1.03	2.87	-	0.32	8	Fe^{2+} Ol		0.87	2.99	-	0.39	3	Fe^{2+} Ol
	1.17	2.92	-	0.32	13	Fe^{2+} Ol		0.35	0.00	47.1	0.50	11	Fe^{3+} Mfr
	0.32	0.00	47.6	0.55	6	Fe^{3+} Mfr		0.34	0.00	44.1	0.50	4	Fe^{3+} Mfr
	0.60	0.00	44.5	0.55	8	Fe^{3+} Mfr		0.37	-0.19	51.7	0.40	26	Fe^{3+} Hem
	0.37	-0.13	49.2	0.55	18	Fe^{3+} Hem		0.37	-0.20	49.4	0.40	16	Fe^{3+} Hem
	0.40	0.90	-	0.65	7	Fe^{3+}		0.43	0.93	-	0.40	10	Fe^{3+}
								0.18	0.54	-	0.40	7	Fe^{3+}

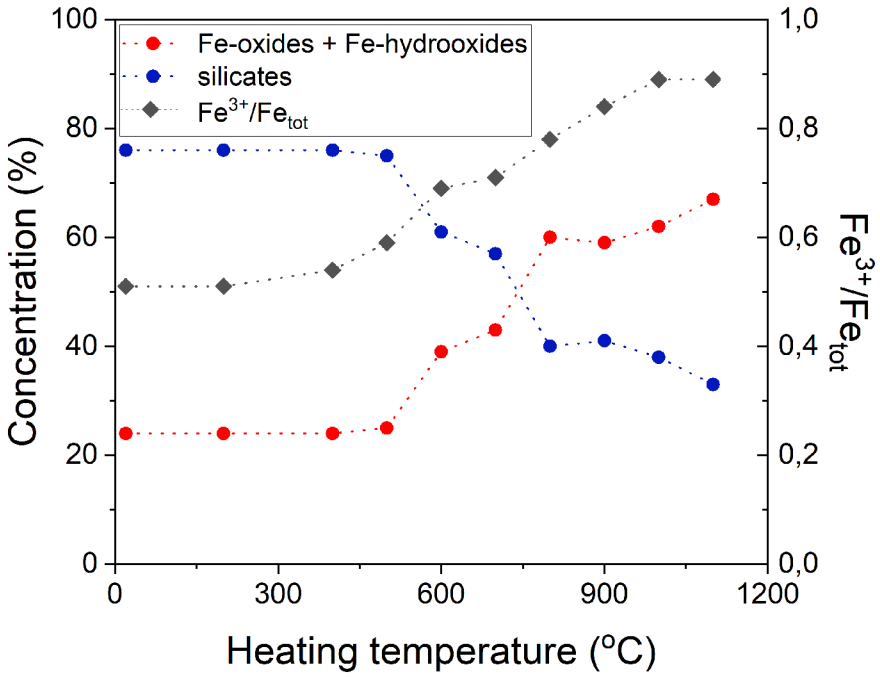

Figure 6. Changes in concentration of silicates, Fe-oxides/hydroxide and ratio of Fe^{3+} to total iron (Fe_{tot}) obtained after heating at high temperatures for basalt 0-2 mm size fraction.

is advancing with an increase in annealing temperature and after annealing the sample above 1000°C only a small amount (~3%) of this mineral was detected on the Mössbauer spectrum. However, olivine diffraction lines are still visible on the X-ray diffractogram after heating the sample to 1000°C. It can suggest that at this temperature we have forsterite in the sample.

Augite structure is much more stable at high temperatures in comparison to olivine (Khisina et al. 2005; Kądziołka-Gaweł et al. 2019). Small changes observed for this compound are oxidation of Fe^{2+} ions to Fe^{3+} ions. However, after heating at 700°C on the Mössbauer spectrum appears a doublet with the values of isomer shift of about 0.16 mm/s and quadrupole splitting 0.45 mm/s, which are characteristic of Fe^{3+} in tetrahedral coordination. This doublet corresponds to ferric ions that can be incorporated in the tetrahedral position, probably, of the augite structure. Note that after heating at 1100°C large concentration of this mineral is still detected. Burkhard (2001) explain the stability of augite during heating in air by diffusion of Ca^{2+} into the sample. She showed that the Ca^{2+} is diffused at the air interface, forming a thin CaO_2 layer that limits the O^{2-} diffusion into the sample's interior. High temperature stability of augite also confirms results of Scorzelli et al. (2005).

Hematite makes up more than 50% of all the iron-bearing phases in the investigated samples of olivine heated above 1000°C (Figure 6, Table 3). However, on Mössbauer spectrum two sextets with hyperfine magnetic fields ~49.5 T and ~51.5 T are visibly connected with this iron oxide. Substitution of foreign-elements in Fe_2O_3 structure may lead to a decrease in hyperfine magnetic field. Because of similar ionic radii of Fe^{3+} and Al^{3+}, and high concentration of Al in the sample, aluminium can substitute to a significant extent iron in the hematite structure and lower the hyperfine field (Murad, Cashion 2004; Osacký et al. 2009). For this reason two sextets related to hematite are present on the spectrum after heating above 1000°C. A heating temperature of 1100°C was the temperature where contribution of iron-oxides was the highest. What is important, hematite concentration has a great influence on the thermal and elastic properties of basalt products, e.g. basalt fiber (Chen et al. 2022).

5. Conclusions

The paper illustrates that Mössbauer spectroscopy is a technique which can characterize iron-containing minerals and their processing. The changes in the Mössbauer spectra reflect various phases of decomposition and transformation. Knowledge about the physicochemical properties, mineralogy and structure at high temperature ranges is important for basalt suitability for industrial applications. The obtained results show that up to a temperature of 500°C changes in contribution of Fe-bearing minerals are nonsignificant. Heating in temperature range from 500°C to 1100°C leads to a systematic increase in contribution of iron oxides at the cost of silicate minerals, like augite and olivine.

Acknowledgements

All investigated samples are facilitated by PGP "BAZALT" SA (Wilków, Poland). This work was supported by the funds granted under the Research Excellence Initiative of the University of Silesia in Katowice. The constructive comments of two anonymous reviewers are gratefully acknowledged.

Conflicts of interest

The authors have no conflicts of interests to declare.

References

Al-Baijat, H., & Benedetti, A. (2013). Comparison between Composite Column Using Limestone and Basalt Concrete. *Open Journal of Civil Engineering, 3*, 1-6. DOI: 10.4236/ojce.2013.31001.

Barcova, K., Mashlan, M., & Martinec, M. (2003). Mössbauer study of transformation mechanism of Fe cations in olivine after thermal treatments in air. *Journal of Radioanalytical and Nuclear Chemistry, 255*(3), 529– 533. DOI: 10.1023/A:1022588500878.

Burkhard, D.J.M. (2001). Crystallization and Oxidation of Kilauea Basalt Glass: Processes during Reheating Experiments. *Journal of Petrology, 42*(3), 507–527. DOI: 10.1093/petrology/42.3.507.

Brown, D.A., Sawicki, J.A., & Sherriff, B.L. (1998). Alteration of microbially precipitated iron oxides and hydroxides. *American Mineralogist, 83*, 1419–1425.

Chen, M., Liu, J., & Wu, Z. (2022). Effect of Fe_2O_3 Concentration on the Properties of Basalt Glasses. *Journal of Natural Fibers, 19*(2), 575-585. DOI: 10.1080/15440478.2020.1758277.

Dyar, M.D., Klima, R., Fleagle, A., & Peel, S. (2013). Fundamental Mössbauer parameters of synthetic Ca-Mg-Fe pyroxenes. *American Mineralogist, 98, 1172–1186.* DOI: 10.2138/am.2013.4333.

Felippi de Lima, L., Zorzi, J., & Cruz, R. (2022), Basaltic glass-ceramic: A short review. *Boletín de la Sociedad Española de Cerámica y Vidrio, 61*, 2-12. DOI: 10.1016/j.bsecv.2020.07.005.

Gialanella, S., Girardi, F., Ischia, G., Lonardelli, I., Mattarelli, M., & Montagna M. (2010). On the goethite to hematite phase transformation. *Journal of Thermal Analysis and Calorimetry, 102*, 867–873. DOI: 10.1007/s10973-010-0756-2.

Gunnlaugsson, H.P., Rasmussen, H., Kristjánsson, L., Steinthorsson, S., Helgason, Ö., Nørnberg, P., Madsen, M.B., & Mørup, S. (2008). Mössbauer spectroscopy of magnetic minerals in basalt on Earth and Mars. *Hyperfine Interactions, 182*, 87–101. DOI: 10.1007/s10751-008-9714-9.

Hassan, K.M. (2015). The Iron Mineralogy of Eocene Fossil Wood - a Mössbauer Study of Samples from the Petrified Forest, New Cairo, Egypt. *The Canadian Mineralogist*, *53*(4), 705–716. DOI: 10.3749/canmin.1400108.

Hassan, K.M., & Dekan, J. (2013). Mössbauer study of Fe phases in terrestrial olivine basalts from southern Egypt. *Mineralogia, 44*(1-2), 3-12. DOI: 10.2478/mipo-2013-0001.

Kądziołka-Gaweł, M., Adamczyk, Z., & Kalinowski, L. (2019). Mössbauer study of changes in olivine after heating in air. *The Canadian Mineralogist, 57*, 105-115. DOI: 10.3749/canmin.1700074.

Kądziołka-Gaweł, M., Dulski, M., Kalinowski, L., & Wojtyniak, M. (2018). The effect of gamma irradiation on the structural properties of olivine. *Journal of Radioanalytical and Nuclear Chemistry, 317*, 261–268. DOI: 10.1007/s10967-018-5849-6.

Khisina, N., Khramov, D., Kolosov, M., Klesehev, A., & Taylor, L.A. (2005). Formation of Ferriolivine and Magnesioferrite from Mg – Fe-Olivine: Reactions and Kinetics of Oxidation. *Physics and Chemistry of Minerals, 22*(4), 241-250. DOI: 10.1007/BF00202257.

Komadel, P., Anastácio, A., Andrejkovičová, S., & Stucki, J. (2008). Iron phases identified in bentonite from the Lieskovec deposit (Slovakia) by variable temperature: Mössbauer spectroscopy. *Clay Minerals, 43*(1), 107–115. DOI: 10.1180/claymin.2008.043.1.08.

Lakshman, A., Subba Raob, P., & Raob, K. (2004). Mössbauer spectroscopic analyses of $Mg_{0.9}Mn_{0.1}In_xFe_{2-x}O_4$ spinel ferrites. *Journal of Magnetism and Magnetic Materials, 284*, 352–357. DOI: 10.1016/j.jmmm.2004.06.058.

Liu, Q., Shaw, M., Parnas, R., & McDonnell, A. (2006). Investigation of Basalt Fiber Composite Mechanical Properties for Applications in Transportation. *Polimer Composites, 27*, 41-48. DOI: 10.1002/pc.20162.

Malczewski, D., Jeleń, M., Żaba, J., Błachowski, A., Ruebenbauer, K., & Dziurowicz, M. (2017). Identification of iron-bearing minerals in basalts and pillow lavas of the Kaczawa mountains using ^{57}Fe Mössbauer spectroscopy. *Nukleonika, 62*(2), 145-148. DOI: 10.1515/nuka-2017-0021.

Monaldo, E., Nerilli, F., & Gairo, G. (2019). Basalt-based fiber-reinforced materials and structural applications in civil Engineering. *Composite Structures, 214,* 246–263. DOI: 10.1016/j.compstruct.2019.02.002.

Morimoto, N. (1988). Nomenclature of Pyroxenes. *Mineralogy and Petrology, 39,* 55-76.

Morozov, M., Brinkmann, Ch., Lottermoser, W., Tippelt, G., Amthauer, G., & Kroll, H. (2005). Octahedral cation partitioning in Mg,Fe^{2+}-olivine. Mössbauer spectroscopic study of synthetic $(Mg_{0.5}Fe^{2+}_{0.5})_2SiO_4$ (Fa_{50}). *European Journal of Mineralogy, 17,* 495-500. DOI: 10.1127/0935-1221/2005/0017-0495.

Murad, E., & Cashion, J. (2004). *Mössbauer spectroscopy of environmental materials and their industrial utilization.* Kluwer Academic Publishers, Norwell, Massachusetts. 417 p.

Osacký, M., Honty, M., Madejová, J., Bakas, T., & Šucha, V. (2009). Experimental interactions of Slovak bentonites with metallic iron. *Geologica Carpathica, 60*(6), 535-543. DOI: 10.2478/v10096-009-0039-7.

Özdemir, Ö., & Dunlop, D. (2000). Intermediate magnetite formation during dehydration of goethite. *Earth and Planetary Science Letters, 177,* 59-67. DOI: 10.1016/S0012-821X(00)00032-7.

Rivas-Sanchez, M.L., Alva-Valdivia, L.M., Arenasalatorre, J., Urrutia-Fucugauchi, J., Perrin, M., Goguitchaichvili, A., Ruiz-Sandoval, M., & Ramos Molina, M.A. (2009). Natural magnetite nanoparticles from an iron-ore deposit: size dependence on magnetic properties. *Earth, Planets and Space, 61*, 151–160. DOI: 10.1186/BF03352895.

Scorzelli, R., Souza Azevedo, I., Stewart, S., Varela, M., & Kurat, G. (2005). Druse Pyroxenes in D'Orbigny: A Mössbauer Spectroscopy Study [Abstract]. AIP Conference Proceedings, 795, 214. DOI: 10.1063/1.2128361.

Sunny, J.E., Varghese, R.A., Sagar, S., John, S., & Kassim, R. (2020). Application of Basalt and its Products in Civil Engineering. *International Journal of Engineering Research & Technology, 9*(6), 511-515.

Sedlačková, K., Sitek, J., & Novák, P. (2021). Analysis of Mount Etna's volcanic rocks. *Journal of Electrical Engineering, 72*, 106–112. DOI: 10.2478/jee-2021-0014.

Stevens, J., Khasanov, A., Miller, J., Pollak, H., & Li, Z. (2005). *Mössbauer Mineral Handbook.* Mössbauer Effect Data Center, Asheville, USA.

Stucki, J.W., Goodman, B.A., & Schwertmann, U. (1988). *Iron in Soils and Clay Minerals.* D. Reidel, Dordrecht, 893 p.

Thompson, A., Rancourt, D.G., Chadwick, O.A., & Chorover, J. (2011). Iron solid-phase differentiation along a redox

gradient in basaltic soils. *Geochimica et Cosmochimica Acta, 75,* 119–133. DOI: 10.1016/j.gca.2010.10.005.

Urbanski, M., Lapko, A., & Garbacz, A. (2013). Investigation on Concrete Beams Reinforced with Basalt Rebars as an Effective Alternative of Conventional R/C Structures. *Procedia Engineering, 57,* 1183-1191. DOI: 10.1016/j.proeng.2013.04.149.

Received: 03 November 2021
Accepted: 27 April 2022
Handling Editor: Abigail Barker